Design and Performance Analysis of Hexagonal Transmon Qubit in a Superconducting Circuit

Seong Hyeon Park, Jeseok Bang, Soobin An, and Seungyong Hahn

***Abstract*—Superconducting quantum bits (qubits) are considered as promising candidates to serve as a platform for a quantum information processor. For the realization of practical quantum computing devices, scalable designs and long lifetimes of qubits are required. In this paper, we present simulation results of "hexagonal" transmon qubit in a superconducting coplanar waveguide (CPW) resonator. We conducted finite-element method simulations considering dielectric losses including the two-level system (TLS) loss to evaluate the performance of the qubit in a practical sense. Then, key parameters of a qubit in superconducting circuits - including lifetime, coupling strength, and energy levels are estimated by the black-box quantization method or by solving circuit quantum-electrodynamics (cQED). Finally, the geometric features and key parameters of the qubit are suggested for typical quantum information processing applications.**

***Index Terms*—Transmon, black-box quantization, circuit QED, superconducting CPW resonator.**

I. Introduction

With the recent experimental demonstration of quantum supremacy [1], the expectation that quantum algorithms can be executed on quantum information processor is not an unrealistic dream anymore. Among many candidates for quantum computing platforms, a superconducting circuit with quantum bits (qubits) has been considered as one of the most promising candidate for the scalable and practical quantum computer with the strengths of artificially tunable and nonlinear characteristics of Josephson junctions (JJs) [2], [3]. However, two-level system (TLS) loss [4] with low power input (about single photon energy level) and at low temperatures is known to be the major limiting factor to the quality factor (Q-factor) of a superconducting resonator or a superconducting qubit [5]–[8]. To mitigate TLS loss, surface treatment method [9], [10], changing the materials with low TLS loss [11] and 3D transmon qubits [12] have been tried and achieved remarkable improvements in qubit lifetimes. Especially, 3D transmon qubits in cavity resonators show longer lifetimes compared to 2D planar transmon qubits [13] by the different strength of the electric field in the regions of layer interfaces and the reduced coupling to the TLS. However, the bulk size of 3D cavity resonator hinders scaling up the number of 3D transmon qubits to operate multi-qubit operation. Therefore, an attention has been brought out regarding the geometry of a 2D planar transmon qubit to achieve longer lifetime with scalable designs.

Manuscript received December 1, 2020. This research was supported in part by Samsung Electronics. *(Corresponding author: S. Hahn)*

S. H. Park, J. Bang, S. An, S. Hahn are with the Department of Electrical and Computer Engineering, Seoul National University, 1 Gwanak-ro, Gwanak-gu, Seoul 08826, South Korea. (e-mail: hahnsy@snu.ac.kr)

In this paper, simulation results of the performance of a hexagonal transmon qubit coupled to a superconducting coplanar waveguide (CPW) resonator are presented. In section II, designs and fundamental parameters of superconducting CPW resonator and the qubit are introduced. To estimate the lifetime of the qubit and the coupling strength, black-box quantization theory [14] and circuit quantum electrodynamics (cQED) analysis are introduced in section III. At last, we compare the loss factors due to TLS layers of the qubit by changing designs focusing on the lifetime improvement.

II. Components in a Superconducting Circuit

A. Superconducting CPW Resonator

Superconducting CPW resonators have advantages [15] with respect to applications in quantum information processing: 1) small size of a few millimeters to operate at microwave frequencies; 2) high internal quality factor (Q_{int}); and 3) strong coupling strength to qubits in cQED demonstrations. At low temperatures far below the critical temperature of a superconductor, the Q_{int} of the superconducting circuits can be expressed as follows [16]:

$$Q_{\mathrm{int}}^{-1} = Q_{\mathrm{qp}}^{-1} + Q_{\mathrm{TLS}}^{-1} + Q_{\mathrm{rad}}^{-1} + \cdots, \tag{1}$$

where Q_{qp}, Q_{TLS}, and Q_{rad} are Q-factors due to quasiparticle losses, TLS losses, and radiation respectively. At low temperatures and small power input, Q_{TLS} can be the major contribution [17] to the loss in low impedance superconducting circuits [18]. Typically, TLS defects are assumed to intensively lie in amorphous substrate-metal (SM), substrate-air (SA), and metal-air (MA) interfaces [19]. At low temperatures with small power input, Q_{TLS} of TLS layer is:

$$Q_{\mathrm{TLS}}^{-1} = Q_{\mathrm{SM}}^{-1} + Q_{\mathrm{SA}}^{-1} + Q_{\mathrm{MA}}^{-1} + Q_{\mathrm{sub}}^{-1}, \tag{2}$$

$$Q_i^{-1} = p_i \tan\delta_i^0, \tag{3}$$

where p_i is the energy participation ratio [20]–[22] and $\tan\delta_i^0$ is the loss tangent of TLS layer of i.

Calculation results of key parameters of superconducting niobium CPW $\lambda/4$-resonator on high pure sapphire substrate operating at 15 mK are shown in Table I. The geometric inductance (L_l), capacitance (C_l) and kinetic inductance (L_k) are calculated through the methods in [16], [23]. Parameters of superconducting niobium and sapphire substrate are taken from [24]–[26] and the TLS parameters of the relative permittivity (ε_r), loss tangent ($\tan\delta^0$) are taken from [27], [28] while the thickness (t) of SM, SA and MA layers are assumed to be 2 nm, 5 nm and 5 nm respectively in this study. We assumed that the sapphire has isotropic properties and the ratio between the

TABLE I
PARAMETERS OF SUPERCONDUCTING NIOBIUM CPW $\lambda/4$-RESONATOR. THE RESONANT FREQUENCY ($\omega_r/2\pi$) IS ASSUMED TO BE 8 GHZ.

Sapphire		**SM Layer**		**SA Layer**		**MA Layer**		**CPW Geometry**		**CPW Parameters**		**TLS Q-factor**	
$\tan\delta_0$	10^{-9}	$\tan\delta_0$	0.0013	$\tan\delta_0$	0.00031	$\tan\delta_0$	0.0015	S	9 [μm]	C_l	162 [pF/m]	Q_{SM}	1.01×10^6
ε_r	11.5	ε_r	11.5	ε_r	9	ε_r	33	W	6 [μm]	L_k	7.70 [nH/m]	Q_{SA}	2.52×10^6
t	500 [μm]	t	2 [nm]	t	5 [nm]	t	5 [nm]	t_{sc}	200 [nm]	L_l	421 [nH/m]	Q_{MA}	2.19×10^7

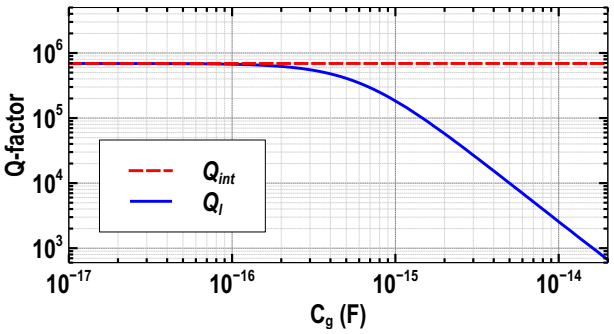

Fig. 1. Q_l of the superconducting Nb CPW $\lambda/4$-resonator as a function of C_g. The dashed line represents the Q_{int} of the resonator which is calculated as 6.9×10^5. Due to the small $\tan\delta_0$ of sapphire, we assumed that the SM, SA and MA layers are the major contributions to the Q_{TLS}.

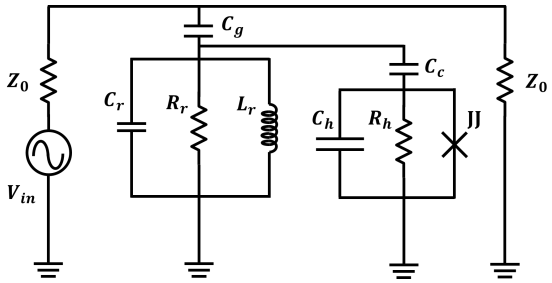

Fig. 2. Lumped element circuit diagram for a transmon qubit and a resonator capacitively coupled to a transmission line. A Josephson junction in the transmon qubit is denoted with "X" symbol. Loss factors of a resonator and a transmon qubit are denoted with R_r and R_h respectively.

center strip width (S) and gap width (W) of superconducting CPW structure is chosen to be 3:2 to match the characteristic impedance (Z_0) of the CPW resonator in a value of 50 Ω while the thickness of superconducting layer (t_{sc}) is fixed as 200 nm. The p_i and corresponding Q_{TLS} are calculated by FEM simulations. When the superconducting CPW resonator is capacitively coupled to a transmission line, the loaded quality factor (Q_l) can be simplified as $Q_l^{-1} = Q_{\mathrm{int}}^{-1} + Q_e^{-1}$, where Q_e is the external Q-factor determined by the choice of the coupling capacitance (C_g) between the transmission line and the CPW resonator. The Q_l of the superconducting Nb CPW $\lambda/4$-resonator in Table I is shown in Fig. 1.

B. Superconducting Transmon Qubit

A novel approach in qubit design to suppress the effect of flux noise by introducing additional shunted capacitor to flux qubit was proposed by J.Q. You *et al* [29] in 2007. Likewise, a transmon qubit is widely used as an artificial two-level system, which has been introduced by J. Koch *et al* [30]. The transmon qubit where Josephson junction (JJ) is coupled to a shunt capacitor (C_h) which exponentially suppresses the charge dispersion while the anharmonicity decreases algebraically. In Fig. 2, a simplified lumped element circuit diagram for a transmon qubit coupled to a resonator is presented. In the dispersive limit when the detuning between the state transition frequency of the qubit and the resonator is significantly larger than the qubit-resonator coupling strength (g), the effective Hamiltonian ($\hat{H}_{\mathrm{eff}}$) of the circuit can be simplified in the rotating wave approximation as follows [31]–[33]:

$$\hat{H}_{\mathrm{eff}} = \hbar(\omega_r + \chi\hat{\sigma}_z)\hat{a}^\dagger\hat{a} + \frac{\hbar}{2}(\omega_{01} + \chi)\hat{\sigma}_z, \tag{4}$$

$$\chi \approx -\frac{g^2 E_C}{\Delta(\Delta - E_C)}, \tag{5}$$

where $\hbar$, E_C, and χ indicate the reduced Planck's constant, charging energy of the qubit, and dispersive shift respectively. The operators of $\hat{a}^\dagger$ and $\hat{a}$ are the annihilation and creation of a photon while $\hat{\sigma}_z$ is Pauli matrix z component. In (5), Δ indicates the differences between the ground to exited state transition angular frequency of a qubit (ω_{01}) and the resonator frequency (ω_r). At transmon regime $E_J/E_C \gg 1$ where E_J is JJ's energy, the n^{th} energy levels of a qubit can be approximated by [30]:

$$E_n \approx -E_J + \sqrt{8E_JE_C}(n+\frac{1}{2}) - \frac{E_C}{12}(6n^2+6n+3). \tag{6}$$

Thus, the anharmonicity (α) can be simplified as $\alpha \approx -E_C$ for the transmon qubit. A transmon qubit is usually realized by interdigitated capacitor [34], parallel pad capacitor [35], Xmon [36], and coaxial capacitor [37]. In this study, we design hexagonal transmon qubit in terms of the simple geometry and compact size to achieve typical E_C. We performed numerical analysis on the qubit to study the surface losses in a hexagonal geometry as shown in Fig. 3. Here, we chose the critical current $I_c = 60$ nA and the junction capacitance $C_J = 1$ fF of JJ for typical values [14], [38]. Then, we designed the qubit to have the charging energy about 200 MHz with the E_J/E_C ratio to be greater than 100. In terms of superconducting circuit analysis, resonant frequency ($\omega_r/2\pi$) of superconducting CPW $\lambda/4$-resonator is chosen to have $\Delta/2\pi \approx 2$ GHz while the gate capacitance C_c between the resonator and the qubit is tuned to have $g/2\pi \approx 90$ MHz by changing g_1 in Fig. 3(b). Parameters of superconducting circuit are derived by black-box quantization theory [14] and compared to cQED analysis.

III. PERFORMANCE ANALYSES OF HEXAGONAL QUBIT

A. Hexagonal Qubit Analysis

We conducted simulations in 3D finite-element-method (FEM) program in consideration of the superconducting char-

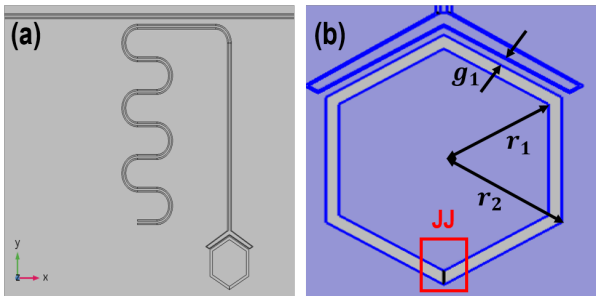

Fig. 3. 3D-modeling in FEM program (COMSOL Multiphysics). (a) The qubit is capacitively coupled to a superconducting CPW $\lambda/4$-resonator. The CPW resonator is capacitively coupled to a transmission line with input and output terminals ($Z_0 = 50\ \Omega$). (b) The inner capacitor is connected to the ground layer by JJ in the qubit. The purple area represents superconducting layer in this figure. r_1 is the inner length and r_2 is the outer length of the hexagonal capacitor. g_1 is the width of the ground superconducting layer between the qubit and the CPW resonator to control the coupling strength.

acteristics of a finite kinetic inductance $L_k \propto 1/\sigma_2$ derived from the complex conductivity (σ_{sc}) [39]:

$$\sigma_{sc}(\omega, T) = \sigma_1 - j\sigma_2, \tag{7}$$

where σ_1 and σ_2 are the real and imaginary part of superconductor's conductivity derived by solving the kernel functions of the Mattis-Bardeen theory [40]. The dielectric parameters of the substrate and TLS layers are chosen as shown in Table I. To consider the losses from thin TLS layers of a few nm scale, we defined boundary interfaces for the TLS layers between the superconducting layers and the bulk substrate/vacuum to avoid the meshing problems and we extracted p_i of the TLS layers by the surface integral of electric field energy on the boundary interfaces respectively with the electromagnetic wave solver. We assumed that the electric field doesn't vary across the thin thickness t of the TLS layers so that p_i can be derived [22]. The p_i of the layers of the qubit as a function of r_1 and r_2 is shown in Fig. 4(b). p_{SM}, p_{SA} and p_{MA} of $r_1 = 110\ \mu$m hexagonal geometry drop about 3, 10 and 2 percents respectively compared to that of $r_1 = 90\ \mu$m geometry.

B. Superconducting Circuit Analysis

To simulate the entire superconducting circuit, thin superconducting layers are modeled with transition boundary condition by imposing $\sigma_{sc}(\omega, T)$ from (7) for 200 nm thickness. To extract the coupling parameters, a lumped port at JJ in the qubit was defined to calculate the admittance of the system (Y_{sys}) as shown in Fig. 3. Then, the total admittance (Y_{tot}) can be derived by adding the admittance of JJ (Y_{JJ}) as follows [14]:

$$Y_{tot} = Y_{sys} + Y_{JJ}, \tag{8}$$

$$Y_{sys} = \sum_p j\omega C_p + \frac{1}{j\omega L_p} + \frac{1}{R_p}; Y_{JJ} = j\omega C_J + \frac{1}{j\omega L_J}, \tag{9}$$

where, L_J is the inductance of JJ. The resonant frequency of the mode p can be determined as $\omega_p = (L_p C_p)^{-1/2}$. The effective resistances (R_p) are given by $R_p = 1/\mathrm{Re}Y(\omega_p)$ and the effective capacitancecs (C_p) are determined as the derivative form of $C_p = \mathrm{Im}Y'(\omega_p)/2$. The effective inductances (L_p)

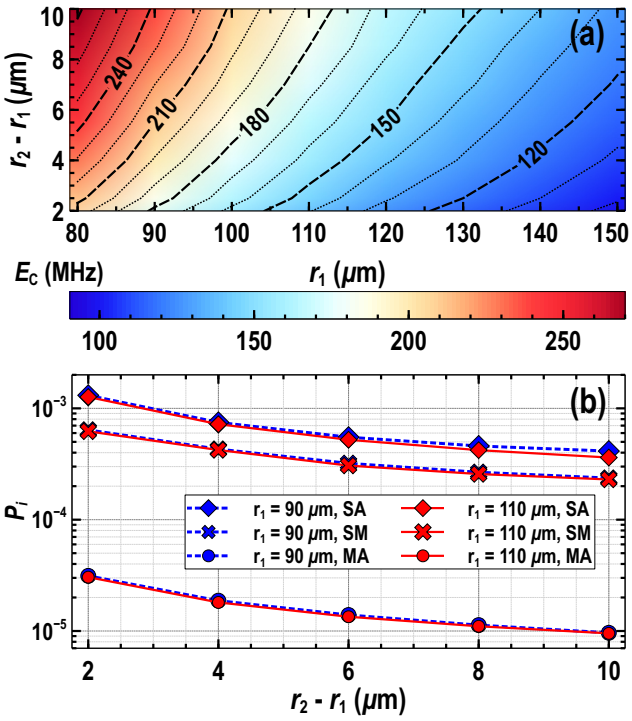

Fig. 4. (a) E_C of hexagonal qubit as a function of geometric parameters of r_1 and $(r_2 - r_1)$. (b) Energy participation ratios of TLS layers. Red solid lines are for r_1 = 110 μm while blue dotted lines are for r_1 = 90 μm geometry.

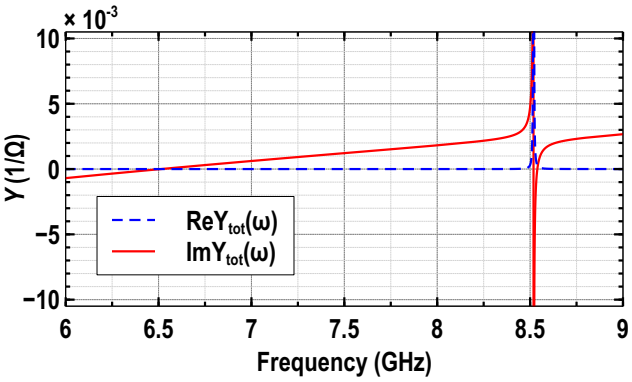

Fig. 5. Real and imaginary parts of the total admittance plot versus frequency. A zero crossing frequency at 6.52 GHz refers to the qubit frequency while the resonant frequency of the CPW resonator occurs at 8.54 GHz.

can be determined from the resonant frequency at mode p. With the definition of the Q-factor for a parallel RLC circuit as $Q = \omega RC$, the Purcell limited Q-factor ($Q_{Purcell}$) can be calculated at the qubit frequency (ω_{qb}). The total admittance from JJ of the qubit of $r_1 = 110\ \mu$m, $r_2 = 120\ \mu$m, and $g_1 = 20\ \mu$m when p_i of TLS layers are minimum is shown in Fig. 5. The dispersive shifts and the anharmonicity can be estimated by the self (χ_{pp}) and cross ($\chi_{pp'}$) Kerr shifts in [14]. The χ_{pp} of mode p and $\chi_{pp'}$ between p and p' can be written as:

$$\chi_{pp} = -\left(\frac{e}{\omega_p C_p \varphi_0}\right)^2 \frac{E_J}{2}; \chi_{pp'} = -2\sqrt{\chi_{pp}\chi_{p'p'}}, \tag{10}$$

TABLE II
KEY PARAMETERS OF THE HEXAGONAL QUBIT COUPLED TO SUPERCONDUCTING CPW $\lambda/4$-RESONATOR IN FIG. 5. VALUES IN () ARE DERIVED BY CQED ANALYSIS.

Parameters		Values	Parameters		Values
E_C	[MHz]	189(188)	Q_l		1.96×10^4
E_J/E_C		157(158)	Q_{SM}		3.35×10^6
$\omega_r/2\pi$	[GHz]	8.54(8.44)	Q_{SA}		7.92×10^6
$\omega_{01}/2\pi$	[GHz]	6.52(6.50)	Q_{MA}		6.55×10^7
$\chi/2\pi$	[kHz]	-494(-526)	$\Gamma^{-1}_{\mathrm{Purcell}}$	[μs]	160(139)
$g/2\pi$	[MHz]	95.4(98.6)	T_1	[μs]	40.9(39.4)

by the relations of charging energy $e^2/2C_J$ and the inductance $L_J=\varphi_0^2/E_J$ of JJ. Here, φ_0 is the reduced flux of quantum and e is the elementary charge. The estimated χ and E_C of the qubit are -494 kHz and 189 MHz respectively which are sufficient to measure the qubit state in the dispersive readout. To verify the key parameters estimated by the black-box quantization theory, we performed cQED analysis. We defined JJ as the lumped element of parallel LC oscillator with L_J and C_J to extract the individual parameters of capacitance and resonant frequency. In the transmon regime, the charging energy of the qubit $E_C=e^2/2C_\Sigma$ where C_Σ is the total capacitance of the qubit. Since the state frequency of the qubit can be approximated as shown in (6), E_C is calculated by solving eigenfrequency study in FEM program. The frequencies of the qubit and the resonator are calculated as 6.50 GHz and 8.44 GHz respecitively. The coupling strength (g) between the qubit and resonator can be derived by the following equation [30]:

$$g=\frac{2}{\hbar}\sqrt{\frac{1}{2}}(\beta eV_{\mathrm{rms}})\left(\frac{E_J}{8E_C}\right)^{1/4}, \tag{11}$$

where $\beta=C_c/C_\Sigma$, the gate capacitance (C_c), and the root-mean-square voltage of the resonator $V_{\mathrm{rms}}=\sqrt{\hbar\omega_r/2C_r}$.

For the superconducting CPW $\lambda/4$-resonator, V_{rms} is calculated as 3.33 μV by using the values in Table I. The gate capacitance (C_c) between the qubit and the resonator is calculated as 3.89 fF by FEM program. By calculating the Q_l of the CPW $\lambda/4$-resonator, the coupling capacitance (C_g) between the transmission line and the CPW $\lambda/4$-resonator can be determined as shown in Fig. 1. Finally, in consideration of various loss channels in a superconducting circuit, T_1 of the qubit can be expressed similar to (1) as [21], [30]:

$$T_1^{-1}=\Gamma_{\mathrm{qp}}+\Gamma_{\mathrm{TLS}}+\Gamma_{\mathrm{Purcell}}+\cdots, \tag{12}$$

$$\Gamma_{\mathrm{Purcell}}=\kappa\frac{g^2}{\Delta^2};\Gamma_{\mathrm{TLS}}=\frac{\omega}{Q_{\mathrm{TLS}}}, \tag{13}$$

where $\Gamma_{\mathrm{Purcell}}$ is the relaxation due to Purcell effect and Γ_{TLS} is the relaxation due to TLS losses. Here, Γ_{qp} is the relaxation due to quasiparticle tunneling effect [41] which is not considered in this study compared to $\Gamma_{\mathrm{Purcell}}$ or Γ_{TLS} for low impedance superconducting circuits at low temperatures. With the coupled resonator decay rate $\kappa=\omega_r/Q_l$, the relaxation due to Purcell effect can be calculated.

To consider the relaxation due to TLS losses, the participation ratios and the corresponding quality factors of SM, SA, MA, and the substrate are calculated by (2). The Q_{TLS} is calculated as 2.27×10^6 corresponding to the relaxation rate due to TLS loss as 55.1 μs. The key parameters of the qubit coupled to the CPW $\lambda/4$-resonator derived by black-box quantization theory and cQED analysis are summarized in Table II.

IV. DISCUSSION

As shown in Table II, The estimated longest lifetime of the qubit ($r_1=110$ μm; $r_2=120$ μm; $g_1=20$ μm) is about 40 μs in consideration of TLS losses from MS, MA, and SA layers. The estimated key parameters of a superconducting circuit composed of the qubit and superconducting CPW $\lambda/4$-resonator show good agreement between the two methods. Comparing T_1 with that of the state-of-the-art qubits [42], further geometry optimizations and adjusting the target coupling parameters are necessary to reduce the energy participations of SM and SA layers which are the major loss contributions of the hexagonal transmon. As shown in Table II, loss due to Purcell effect also contributes to the overall T_1 fairly. Thus, suppressing the loss due to Purcell effect should be achieved. For example, Purcell effects can be effectively avoided without mitigating the qubit quantum nondemolition readout [43] or a bandpass Purcell filter can be used to allow fast measurement without increasing the environmental loss with a transmission line stub by matching the admittance value as purely imaginary as possible [44], [45]. Besides, the lifetimes of qubits can be further improved by changing the superconducting materials or the bulk substrate. Recent study [46] has shown that the superconducting titanium-nitride (TiN) on high pure silicon (Si) substrate has relatively smaller TLS loss factors compared to superconducting niobium on sapphire substrate. The dielectric loss tangents of MS, MA, and SA layers of TiN-Si structure are reported [46] as $\tan\delta^0{}_{\mathrm{SM}}=(4.8\pm2)\times10^{-4}$, $\tan\delta^0{}_{\mathrm{SA}}=(1.7\pm0.4)\times10^{-3}$ and $\tan\delta^0{}_{\mathrm{MA}}=(3.3\pm0.4)\times10^{-4}$ while $\varepsilon_{\mathrm{SM}}=11.4\varepsilon_0$, $\varepsilon_{\mathrm{SA}}=4\varepsilon_0$, $\varepsilon_{\mathrm{MA}}=10\varepsilon_0$ and the thickness of all TLS layers are assumed to be 2 nm. The Q_{TLS} of TiN-Si hexagonal qubits is 3.13×10^6 so that the estimated $\Gamma^{-1}_{\mathrm{TLS}}$ by (13) is about 76.7 μs which is about 1.5 times of that of the current superconducting niobium on sapphire structure. Besides, by etching the substrate layer exposed to the vacuum, it is possible to control the participation ratio of TLS layers [47]. Therefore, the lifetime of hexagonal qubits can be improved with different materials and geometries by changing the target resonant frequency and the coupling strength.

V. CONCLUSION

In this paper, we studied hexagonal transmon qubit designs with a sufficiently large lifetime about 40 μs compared to traditional transmon qubit designs such as Xmon or interdigitated capacitor qubit. With a simple but small size of hexagonal design, not only the possibility of building a scalable quantum circuit but also conducting quantum emulation of a spin system [48] or memories [49] can be expected. Further explorations of optimizing the design and materials are required to be a good candidate for the next generation of multi-qubit quantum information processing devices.

REFERENCES

[1] F. Arute *et al.*, "Quantum supremacy using a programmable superconducting processor," *Nature*, vol. 574, no. 7779, pp. 505–510, 2019.

[2] X. Gu, A. F. Kockum, A. Miranowicz, Y.-x. Liu, and F. Nori, "Microwave photonics with superconducting quantum circuits," *Phys. Rep.*, vol. 718, pp. 1–102, 2017.

[3] A. F. Kockum and F. Nori, "Quantum bits with josephson junctions," in *Fundamentals and Frontiers of the Josephson Effect*. Springer, 2019, pp. 703–741.

[4] P. W. Anderson, B. Halperin, and C. M. Varma, "Anomalous low-temperature thermal properties of glasses and spin glasses," *Philos. Mag.*, vol. 25, no. 1, pp. 1–9, 1972.

[5] C. Müller, J. Lisenfeld, A. Shnirman, and S. Poletto, "Interacting two-level defects as sources of fluctuating high-frequency noise in superconducting circuits," *Phys. Rev. B*, vol. 92, no. 3, p. 035442, 2015.

[6] J. Gao *et al.*, "Experimental evidence for a surface distribution of two-level systems in superconducting lithographed microwave resonators," *Appl. Phys. Lett.*, vol. 92, no. 15, p. 152505, 2008.

[7] D. Niepce, J. J. Burnett, M. G. Latorre, and J. Bylander, "Geometric scaling of two-level-system loss in superconducting resonators," *Supercond. Sci. Technol.*, vol. 33, no. 2, p. 025013, 2020.

[8] J. M. Gambetta *et al.*, "Investigating surface loss effects in superconducting transmon qubits," *IEEE Trans. Appl. Supercond*, vol. 27, no. 1, pp. 1–5, 2016.

[9] A. D. O'Connell *et al.*, "Microwave dielectric loss at single photon energies and millikelvin temperatures," *Appl. Phys. Lett.*, vol. 92, no. 11, p. 112903, 2008.

[10] A. Bruno, G. De Lange, S. Asaad, K. Van Der Enden, N. Langford, and L. DiCarlo, "Reducing intrinsic loss in superconducting resonators by surface treatment and deep etching of silicon substrates," *Appl. Phys. Lett.*, vol. 106, no. 18, p. 182601, 2015.

[11] J. Goetz *et al.*, "Loss mechanisms in superconducting thin film microwave resonators," *J. Appl. Phys.*, vol. 119, no. 1, p. 015304, 2016.

[12] H. Paik *et al.*, "Observation of high coherence in Josephson junction qubits measured in a three-dimensional circuit qed architecture," *Phys. Rev. Lett.*, vol. 107, no. 24, p. 240501, 2011.

[13] C. Rigetti *et al.*, "Superconducting qubit in a waveguide cavity with a coherence time approaching 0.1 ms," *Phys. Rev. B*, vol. 86, no. 10, p. 100506, 2012.

[14] S. E. Nigg *et al.*, "Black-box superconducting circuit quantization," *Phys. Rev. Lett.*, vol. 108, no. 24, p. 240502, 2012.

[15] M. Göppl *et al.*, "Coplanar waveguide resonators for circuit quantum electrodynamics," *J. Appl. Phys.*, vol. 104, no. 11, p. 113904, 2008.

[16] R. Simons and R. N. Simons, *Coplanar waveguide circuits, components, and systems*. Wiley Online Library, 2001, vol. 15.

[17] C. R. H. McRae *et al.*, "Dielectric loss extraction for superconducting microwave resonators," *Appl. Phys. Lett.*, vol. 116, no. 19, p. 194003, 2020.

[18] D. Ristè, C. Bultink, M. Tiggelman, R. Schouten, K. Lehnert, and L. DiCarlo, "Millisecond charge-parity fluctuations and induced decoherence in a superconducting transmon qubit," *Nat. Commun.*, vol. 4, no. 1, pp. 1–6, 2013.

[19] M. Sandberg *et al.*, "Etch induced microwave losses in titanium nitride superconducting resonators," *Appl. Phys. Lett.*, vol. 100, no. 26, p. 262605, 2012.

[20] C. E. Murray, J. M. Gambetta, D. T. McClure, and M. Steffen, "Analytical determination of participation in superconducting coplanar architectures," *IEEE Trans. Microw. Theory Tech.*, vol. 66, no. 8, pp. 3724–3733, 2018.

[21] J. Wenner *et al.*, "Surface loss simulations of superconducting coplanar waveguide resonators," *Appl. Phys. Lett.*, vol. 99, no. 11, p. 113513, 2011.

[22] C. Wang *et al.*, "Surface participation and dielectric loss in superconducting qubits," *Appl. Phys. Lett.*, vol. 107, no. 16, p. 162601, 2015.

[23] D. M. Sheen, S. M. Ali, D. E. Oates, R. S. Withers, and J. Kong, "Current distribution, resistance, and inductance for superconducting strip transmission lines," *IEEE Trans. Appl. Supercond.*, vol. 1, no. 2, pp. 108–115, 1991.

[24] T. Tai, B. G. Ghamsari, T. Bieler, and S. M. Anlage, "Nanoscale nonlinear radio frequency properties of bulk Nb: Origins of extrinsic nonlinear effects," *Phys. Rev. B*, vol. 92, no. 13, p. 134513, 2015.

[25] V. Braginsky, V. Ilchenko, and K. S. Bagdassarov, "Experimental observation of fundamental microwave absorption in high-quality dielectric crystals," *Phys. Lett. A*, vol. 120, no. 6, pp. 300–305, 1987.

[26] D. S. Linden, T. P. Orlando, and W. G. Lyons, "Modified two-fluid model for superconductor surface impedance calculation," *IEEE Trans. Appl. Supercond.*, vol. 4, no. 3, pp. 136–142, 1994.

[27] K. Z. Rajab *et al.*, "Broadband dielectric characterization of aluminum oxide (Al2O3)," *J. Microelectron. Electron. Packag.*, vol. 5, no. 1, pp. 2–7, 2008.

[28] C. Kaiser *et al.*, "Measurement of dielectric losses in amorphous thin films at gigahertz frequencies using superconducting resonators," *Supercond. Sci. Techno.*, vol. 23, no. 7, p. 075008, 2010.

[29] J. You, X. Hu, S. Ashhab, and F. Nori, "Low-decoherence flux qubit," *Phys. Rev. B*, vol. 75, no. 14, p. 140515, 2007.

[30] J. Koch *et al.*, "Charge-insensitive qubit design derived from the Cooper pair box," *Phys. Rev. A*, vol. 76, no. 4, p. 042319, 2007.

[31] R. Bianchetti *et al.*, "Dynamics of dispersive single-qubit readout in circuit quantum electrodynamics," *Phys. Rev. A*, vol. 80, no. 4, p. 043840, 2009.

[32] A. Blais, R.-S. Huang, A. Wallraff, S. M. Girvin, and R. J. Schoelkopf, "Cavity quantum electrodynamics for superconducting electrical circuits: An architecture for quantum computation," *Phys. Rev. A*, vol. 69, no. 6, p. 062320, 2004.

[33] A. Wallraff *et al.*, "Strong coupling of a single photon to a superconducting qubit using circuit quantum electrodynamics," *Nature*, vol. 431, no. 7005, pp. 162–167, 2004.

[34] A. D. Córcoles *et al.*, "Protecting superconducting qubits from radiation," *Appl. Phys. Lett.*, vol. 99, no. 18, p. 181906, 2011.

[35] J. M. Chow *et al.*, "Implementing a strand of a scalable fault-tolerant quantum computing fabric," *Nat. Commun.*, vol. 5, no. 1, pp. 1–9, 2014.

[36] A. Dunsworth *et al.*, "Characterization and reduction of capacitive loss induced by sub-micron Josephson junction fabrication in superconducting qubits," *Appl. Phys. Lett.*, vol. 111, no. 2, p. 022601, 2017.

[37] J. Rahamim *et al.*, "Double-sided coaxial circuit QED with out-of-plane wiring," *Appl. Phys. Lett.*, vol. 110, no. 22, p. 222602, 2017.

[38] T. Lindström, C. Webster, J. Healey, M. Colclough, C. Muirhead, and A. Y. Tzalenchuk, "Circuit QED with a flux qubit strongly coupled to a coplanar transmission line resonator," *Supercond. Sci. Techno.*, vol. 20, no. 8, p. 814, 2007.

[39] S. Zhou, A. Jabbar, J. S. Bao, K. Wu, and B. Jin, "Analytical solution of Mattis–Bardeen theory for surface impedance of superconductors," *J. Appl. Phys.*, vol. 71, no. 6, pp. 2789–2794, 1992.

[40] D. Mattis and J. Bardeen, "Theory of the anomalous skin effect in normal and superconducting metals," *Phys. Rev.*, vol. 111, no. 2, p. 412, 1958.

[41] R. Lutchyn, L. Glazman, and A. Larkin, "Kinetics of the superconducting charge qubit in the presence of a quasiparticle," *Phys. Rev. B*, vol. 74, no. 6, p. 064515, 2006.

[42] A. Nersisyan *et al.*, "Manufacturing low dissipation superconducting quantum processors," in *IEEE International Electron Devices Meeting (IEDM)*. IEEE, 2019, pp. 31.1.1–31.1.4.

[43] X. Wang, A. Miranowicz, and F. Nori, "Ideal quantum nondemolition readout of a flux qubit without Purcell limitations," *Phys. Rev. Appl.*, vol. 12, no. 6, p. 064037, 2019.

[44] E. Jeffrey *et al.*, "Fast accurate state measurement with superconducting qubits," *Phys. Rev. Lett.*, vol. 112, no. 19, p. 190504, 2014.

[45] E. A. Sete, J. M. Martinis, and A. N. Korotkov, "Quantum theory of a bandpass Purcell filter for qubit readout," *Phys. Rev. A*, vol. 92, no. 1, p. 012325, 2015.

[46] W. Woods *et al.*, "Determining interface dielectric losses in superconducting coplanar-waveguide resonators," *Phys. Rev. Appl.*, vol. 12, no. 1, p. 014012, 2019.

[47] G. Calusine *et al.*, "Analysis and mitigation of interface losses in trenched superconducting coplanar waveguide resonators," *Appl. Phys. Lett.*, vol. 112, no. 6, p. 062601, 2018.

[48] J. You, X.-F. Shi, X. Hu, and F. Nori, "Quantum emulation of a spin system with topologically protected ground states using superconducting quantum circuits," *Phys. Rev. B*, vol. 81, no. 1, p. 014505, 2010.

[49] A. Zagoskin, S. Ashhab, J. Johansson, and F. Nori, "Quantum two-level systems in josephson junctions as naturally formed qubits," *Phys. Rev. Lett.*, vol. 97, no. 7, p. 077001, 2006.